JGR Earth Surface

RESEARCH ARTICLE
10.1029/2021JF006352

The Fate of Sediment After a Large Earthquake

Oliver Francis[1,2,3], Xuanmei Fan[4], Tristram Hales[1,2,5], Daniel Hobley[2], Qiang Xu[4], and Runqiu Huang[4]

[1]Sustainable Places Research Institute, Cardiff University, Cardiff, UK, [2]School of Earth and Environmental Sciences, Cardiff University, Cardiff, UK, [3]Now at Section 4.7: Earth Surface Process Modelling, German Research Centre for Geosciences (GFZ), Potsdam, Germany, [4]State Key Laboratory for Geohazard Prevention and Geoenvironment Protection, Chengdu University of Technology, Chengdu, China, [5]RSK ADAS Ltd, Helsby, Cheshire, UK

Abstract Large earthquakes rapidly denude hillslopes by triggering thousands of coseismic landslides. The sediment produced by these landslides is initially quickly mobilised from the landscape by an interconnected cascade of processes. This cascade can dramatically but briefly enhance local erosion rates. Hillslope and channel processes, such as landsliding and debris flows, interact to influence the total mass, caliber, and rate of sediment transport through catchments. Calculating the sediment budget of an earthquake lends insight into the nature of these interactions. Using satellite imagery derived landslide inventories, channel surveys and a literature review combined with a Monte Carlo simulation approach we present a constrained sediment budget of the first decade after the 2008 M_w7.9 Wenchuan earthquake. With this sediment budget we demonstrate that debris flows are dominant process for delivering sediment into channels and that large volumes of sediment remain in the landscape. In our study area over 88% (469.7 Mega tonnes) of the coseismically generated sediment remains on the hillslopes in 2018. Of the 12% of the sediment that was mobilised, 67% (45.2 ± 22 Mt) was mobilised by debris flows. Despite the large proportion of sediment remaining on the hillslope, the frequency of debris flows declined significantly over our observation period. The reduction in debris-flow frequency is not correlated to reductions in the frequency of triggering storms, suggesting changes in the mechanical properties of hillslope sediment may drive this observation. The stabilization of coseismically generated sediment greatly extends its residence time and may influence catchment sediment yields for centuries or millennia.

Plain Language Summary Earthquakes produce large volumes of sediment by triggering landslides in mountain ranges. After many earthquakes there is an order-of-magnitude increase in erosion rates, however this period of enhanced erosion is short lived. Understanding the processes which control the timespan of the elevated erosion rates and the rates at which they move sediment is vital for determining the continuing impact the earthquake has on a landscape. Using satellite imagery to map and track the movement of sediment after the 2008 Wenchuan earthquake we show that more than 88% (469.7 mega tonnes) of the sediment produced by the earthquake remains on the hillslope after a decade. Debris flows initiating in the landslide deposits are responsible for most of the erosion during this time. The frequency of these flows decreases rapidly after the earthquake indicating the sediment can stabilize quickly. The stabilized sediment could reside in the mountain range for hundreds or thousands of years indicating that it could have a significant impact on erosion rates and landscape evolution.

Key Points:

- More than 88% (469.7 Mt) of sediment produced by the 2008 M_w7.9 Wenchuan earthquake remains on the hillslope 10 years after the event
- Debris flows rather than fluvially driven erosion are the key process in transporting sediment from the hillslope into the main river
- Evacuation of landslide deposits is highly stochastic indicating the need for long observation periods to estimate residence time

Supporting Information:

Supporting Information may be found in the online version of this article.

Correspondence to:

O. Francis,
Oliver.Francis@gfzpotsdam.de

Citation:

Francis, O., Fan, X., Hales, T., Hobley, D., Xu, Q., & Huang, R. (2022). The fate of sediment after a large earthquake. *Journal of Geophysical Research: Earth Surface*, *127*, e2021JF006352. https://doi.org/10.1029/2021JF006352

Received 12 JUL 2021
Accepted 22 FEB 2022

Author Contributions:

Conceptualization: Oliver Francis, Xuanmei Fan, Tristram Hales, Daniel Hobley
Funding acquisition: Qiang Xu, Runqiu Huang
Methodology: Oliver Francis, Xuanmei Fan, Tristram Hales, Daniel Hobley
Project Administration: Qiang Xu, Runqiu Huang
Supervision: Xuanmei Fan, Tristram Hales, Daniel Hobley
Writing – review & editing: Oliver Francis, Xuanmei Fan, Tristram Hales

1. Introduction

Large, continental earthquakes can produce thousands of coseismic landslides eroding several cubic kilometres of sediment from the hillslopes of tectonically active mountain ranges (Keefer, 2002; Malamud et al., 2004). Coseismic landsliding potentially accounts for over 50% of long term erosion rates in these mountains (G. Li et al., 2014, 2017; Marc, Hovius, & Meunier, 2016; Marc, Hovius, Meunier, Gorum, & Uchida, 2016). Understanding how earthquakes affect the evolution of landscapes requires a consideration of both the direct impact of the landslides on hillslopes and how the erosion or storage of the sediment impacts the evolution of the channel network (Campforts et al., 2020; Egholm et al., 2013). Coseismic landslides reduce the relief of steep hillslopes and can alter the size of drainage basins via erosion of basin ridges (Dahlquist et al., 2018; Schmidt & Montgomery, 1995). Furthermore landslide deposits contribute to debris flow generation (Fan, Scaringi, Korup, et al., 2019) and provide tools or cover for abrading/protecting the bedrock channels altering the evolution of

upland rivers (Egholm et al., 2013; Turowski & Rickenmann, 2009; Yanites et al., 2010). Long term storage of the coseismically generated sediment can dampen the isostatic response of an earthquake (Densmore et al., 2012) or reduce the bedrock erosion of future earthquakes (Francis et al., 2020; G. Li et al., 2014; Marc, Hovius, & Meunier, 2016; Stolle et al., 2019). Therefore, to fully incorporate earthquakes into models of landscape evolution we must understand the processes and timescales by which coseismically generated sediment is exported from orogens. Key to this aim is fully understanding and quantifying the erosional processes which mobilize coseismically generated sediment following earthquakes.

Following large earthquakes it is typical (though not ubiquitous; Tolorza et al., 2019) to see an order-of-magnitude increase in sediment discharge in orogen draining rivers (Dadson et al., 2004; Hovius et al., 2011, 2000; Pain & Bowler, 1973; J. Wang et al., 2015). However, this period of elevated erosion is generally short lived, typically lasting less than a decade, resulting in significant, but unquantified, volumes of sediment remaining in the orogen after sediment discharges have returned to previous levels. As many coseismic landslides occur in bedrock much of the sediment within their deposits is too coarse to be transported by suspension resulting in aggradation of channels for decades after an earthquake (Koi et al., 2008; Pearce & Watson, 1986; Vanmaercke et al., 2017). This coarse sediment must be transported by bedload processes and is likely to remain in the landscape for hundreds of years. Empirical estimates of bedload transport estimate that the sediment from the 1999 Chi Chi earthquake in Taiwan could take 250–600 years to be fully evacuated from the landscape (Yanites et al., 2010). Detailed dating and mapping of the Pokhara region in Nepal also suggests river systems can rework sediment from large earthquakes for several hundred years (Schwanghart et al., 2016; Stolle et al., 2017, 2019).

Alongside the residence time of sediment in the fluvial system, we must also consider possible storage of sediment on the hillslopes. Small landslide deposits can be deposited on the hillslope far from the river or deposited in channels which lack the discharge to consistently erode them (G. Li et al., 2016; Pearce & Watson, 1986; Roback et al., 2018). Landslides disconnected from the channel network cannot be actively reworked by undercutting and therefore must be eroded into the channel network by diffusive processes or stochastically by debris flows, which could significantly increase their residence times (Fan, Scaringi, Korup, et al., 2019; Vanmaercke et al., 2014; S. Zhang & Zhang, 2017). Attempting to include connectivity in dynamic models of sediment transport is difficult due to the rates and initiation mechanisms of these processes being unknown in many locations. However, simple statistical numerical modeling suggests that unconnected landslide deposits could extend the period of time impacted by the earthquake by hundreds or thousands of years (Croissant et al., 2019; Francis et al., 2020).

Satellite imagery with high spatial and temporal resolution allows for the monitoring of large areas of mountain ranges. These can be used to generate multi-temporal landslide inventories after major earthquakes to understand the spatio-temporal evolution of post-seismic mass wasting processes (Kincey et al., 2021; Marc et al., 2015; Chenxiao Tang et al., 2016; S. Zhang & Zhang, 2017). Multi-temporal inventories can provide a link between long term sedimentary (Stolle et al., 2019) and short term suspended sediment discharge records (Lin et al., 2008) by helping to identify the key sediment transport processes. Here we use multitemporal landslide and channel width inventories of the epicentral area of the 2008 M_w 7.9 Wenchuan earthquake to generate the first sediment budget of a large earthquake. These 2 inventories, combined with a literature review, allow us to account for the sources, transport and storage of sediment produced during and in the 10 years following the earthquake (Dietrich et al., 1982; Hinderer, 2012). We use this sediment budget to determine the key sediment transport processes in the post-seismic landscape and to pose questions about the long-term evolution of the epicentral area.

1.1. The Longmen Shan and the 2008 M_w7.9 Wenchuan Earthquake

On 12 May 2008 the Wenchuan region, Sichuan, China, was shaken by a M_w7.9 earthquake with both thrust and dextral strike-slip components. The earthquake occurred along the Longmen Shan thrust zone, which separates the Longmen Shan mountain range from the Sichuan Basin, and ruptured 2 major faults (Figure 1; Densmore et al., 2010; Liu-Zeng et al., 2009). The earthquake triggered more than 60,000 landslides across an area of 35,000 km^2 (Huang & Fan, 2013; G. Li et al., 2014) making it one of the most erosive earthquakes on record (Marc, Hovius, Meunier, Gorum, & Uchida, 2016). Coseismic landsliding is found in the greatest densities on the fault's hanging wall close to the traces of the ruptured faults with areal densities of up to 9.6% (Dai et al., 2011). Areas around the fault zone have weaker rock strength than expected of fresh bedrock (Gallen et al., 2015) and higher denudation rates than the rest of the landscape, suggesting frequent earthquakes have conditioned the area resulting in rapid erosion rates (G. Li et al., 2017).

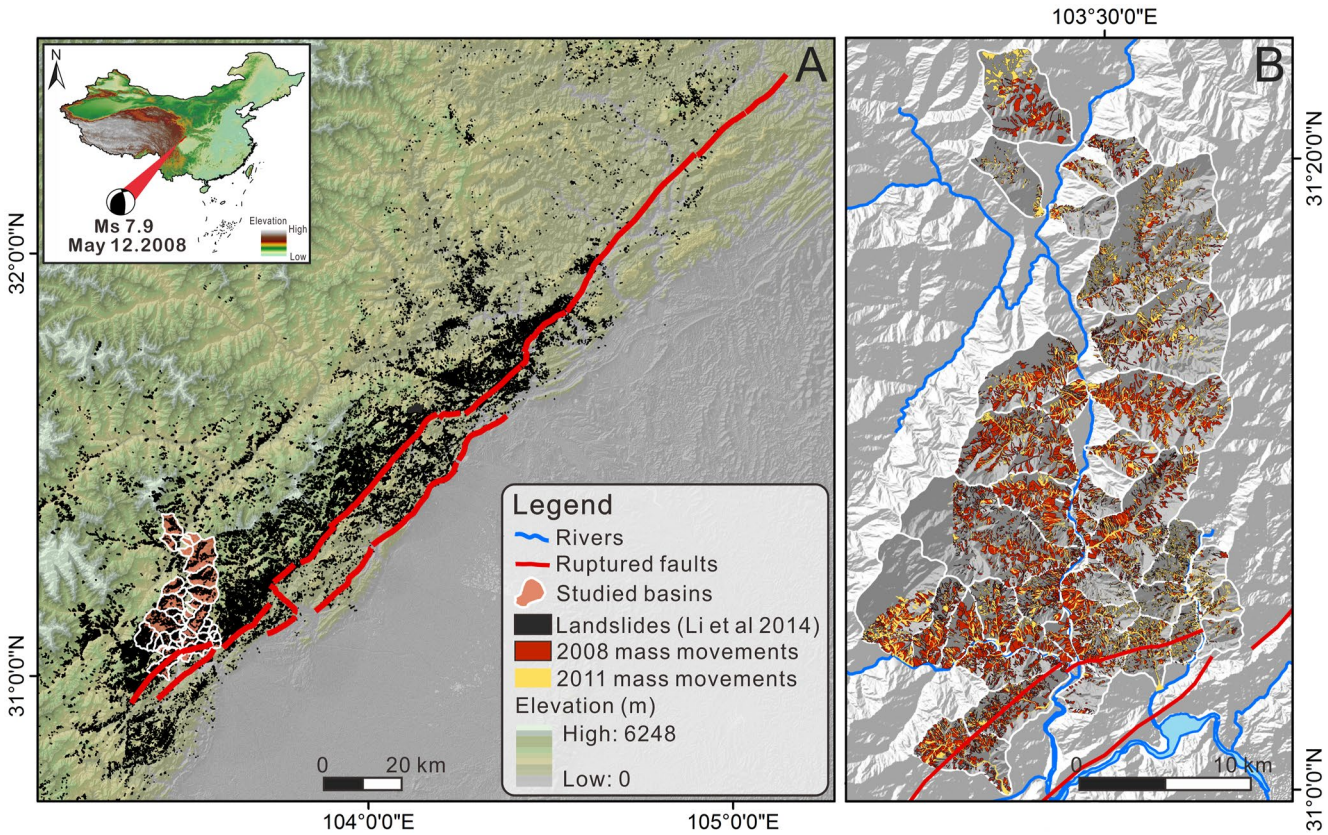

Figure 1. (a) A map of the area affected by the Wenchuan Earthquake. The coseismic landslides mapped by Li et al., 2014 are shown in black while our studied catchments are shown in red with white outlines. The surface expression of the ruptured faults is shown as thick red lines. (b) A focus on our study area with the mapped coseismic and the post-seismic mass movements of 2008–2011 mapped in red and yellow respectively. The main trunk of the Min Jiang is highlighted in blue and all the mapped sub-catchments flow into this river. An example of a mapped catchment can be found in Figure S1 in Supporting Information S1.

The Longmen Shan is one of the steepest mountain ranges in the world, the frontal range rapidly increases in elevation from 500 to 4,000 m over distances of just 50 km (Kirby & Ouimet, 2011). The mountain range is the eastern margin of the Tibetan Plateau in an area of complex tectonic and geodynamic activity (Burchfiel et al., 2008; Hubbard & Shaw, 2009; Royden et al., 2008). The high mountain peaks are dissected by deeply incised valleys and gorges of the rivers draining the mountain range (Densmore et al., 2007; Kirby & Ouimet, 2011). The Min Jiang, the major river draining the epicentral area, is bordered with several layers of terraces which record the long-term uplift and incision of the area (Godard et al., 2010). The main trunk of the river has a characteristic width of 100 m while many of the tributary catchments which drain into the river in the epicentral region of the earthquake are significantly smaller (Figure 1b). Rainfall is highly variable across the mountain range with the highest annual precipitation (800–1,200 mm) found right on the mountain front (Guo et al., 2016). Rainfall and river discharge also vary temporally, the monsoon season between May and October is responsible for the majority of the rainfall and discharge (J. Wang et al., 2015). Mass movements are common in the Longmen Shan due to the steep hillslopes and high frequency of intense rain storms in the mountain range (Ouimet et al., 2007, 2009).

Following the earthquake, coseismic landslide sediment was immediately eroded and reworked by the fluvial system. Suspended sediment discharges in the Min Jiang and other rivers, increased by an order of magnitude (J. Wang et al., 2015), while the concentrations of cosmogenic ^{10}Be in detrital sediment dramatically declined (W. Wang et al., 2017; West et al., 2014). On average these records show that after an initial rapid increase just after the earthquake sediment transport has or is returning rapidly to pre-earthquake levels. However, there is significant variation in this pattern which is primarily linked to the landslide density in individual catchments. Catchments with higher landslide densities and more frequent large rainstorms tend to produce larger and longer lasting increases in sediment discharge (J. Wang et al., 2015; W. Wang et al., 2017). These increases seem to be unaffected by the volume of sediment connected to channel network. Here connection defines the location

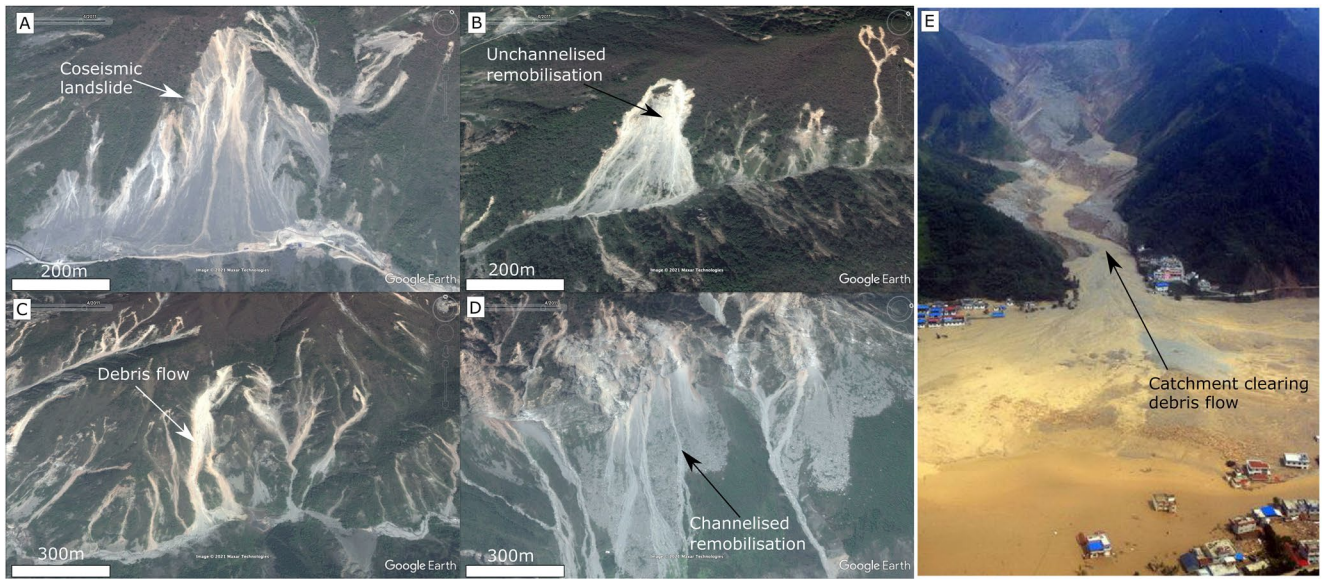

Figure 2. Examples of sediment remobilization observed in the epicentral area of the Wenchuan earthquake. (a) shows a coseismic landslide. (b) shows a very active landslide which is being remobilized in many hard to delineate areas, we term this unchannelised remobilization. C, D, and E all show different types of debris flow. C are primarily "new" debris flows which only mobilize minimal amounts of previously deposited sediment, D are channelized remobilization which are debris flows which mobilize significant volumes of coseismic sediment during their runout. E is an example of a catchment clearing debris flow, these are the largest single events recorded in the area and transport large volumes of sediment from the tributary catchments directly into the main trunk of the Min Jiang. Panels A, B, C and D are producing using imagery from Google Earth and Maxar Technologies. E is an aerial photo of the Wenjia catchment in Wenchuan county taken from Tang et al., 2012.

of the landslide deposit in relation to the channel network. Any landslide that is deposited into the channel network is deemed connected. Around 40% of the total coseismic landslide sediment volume is connected to the channel network but suspended sediment discharge remains high even in locations with low connectivity (G. Li et al., 2016). The lack of a correlation between suspended sediment discharge and connectivity could be an indicator of the high mobility of fine sediment immediately after the earthquake (Figure 2).

The most striking indicator of the earthquake significantly impacting the sediment transport rates of the area is the occurrence of huge (mobilizing $>10^6$ m^3 of sediment) debris flows (C. Tang et al., 2012; Figure 2e). These are some of the largest debris flows ever observed and have occurred with frequencies rarely seen elsewhere (Korup, 2012). The debris flows mostly occurred in the smaller tributary catchments of the Min Jiang where high landslide densities are common and significant aggradation of the channel bed is observed (S. Zhang & Zhang, 2017; Figure 2b). Large debris flows are likely to be single largest part of the stochastic sediment cascades (Bennett et al., 2014; S. Zhang & Zhang, 2017). Understanding these events in the context of other smaller processes in a sediment budget is important to determine the likely future evolution of risk and landscape processes in the region.

2. Materials and Methods

2.1. Study Area

Our sediment budget is focused upon the Min Jiang as it passes through the epicentral region of the Wenchuan earthquake (Figure 1). The study area is made up of 28 sub-catchments which discharge directly into the main trunk of the Min Jiang (Figure 1b). The boundaries of the sub-catchments are defined by a flow direction algorithm and typically have a Strahler stream order of less than 4. This area was one of the most strongly affected by the earthquake, with widespread landsliding dramatically hampering recovery efforts (Chuan Tang & Van Westen, 2018). Approximately 10% of the total coseismic landsliding volume is generated and stored in these catchments which represent 1.2% of the total area affected by the earthquake (Fan, Scaringi, Domènech, et al., 2019; G. Li et al., 2014). The landslides were triggered on the steep hillslopes with an aerial density of up to 9.6% (Dai et al., 2011). The loose sediment of the landslide deposits was eroded during subsequent monsoon seasons, with catchment clearing debris flows occurring in 2008, 2010, 2013, and 2019. The largest catchment

clearing debris flow blocked the Min Jiang causing the river to flood and damage the recovering town of Yingxiu (Chuan Tang et al., 2011).

This area offers an excellent opportunity to study the sediment dynamics of a post seismic landscape due to the high density of landsliding and rapid erosion rates. The suspended sediment load in the Min Jiang suggests erosion rates increased by an order of magnitude while the nearby Zipingpu reservoir offers an opportunity to analyze the impact of the earthquake on a local sink (J. Wang et al., 2015; F. Zhang et al., 2019). Field observations indicate that despite the high erosion rates large volumes of sediment still remain in the area trapped on the hillslopes and within the channel deposits of the tributary sub-catchments.

The study area is well served by high resolution satellites with frequent cloud free imagery allowing for multiple repeat surveys of the hillslopes and channels. We use these images and previously published landslide inventories (Fan, Scaringi, Domènech, et al., 2019) to construct our multi-temporal mass movement and channel width inventories. We then use previously published databases of large debris flow events (Fan, Scaringi, Domènech, et al., 2019), suspended sediment discharge (J. Wang et al., 2015), and field records of overland flow erosion to produce a complete sediment budget (Fusun et al., 2013).

2.2. Construction of the Sediment Budget

Our sediment budget is focused on constraining the volume of sediment generated, stored and eroded from the tributary catchments of the Min Jiang within the epicentral area of the Wenchuan earthquake (Figure 1b). For all tributary catchments in our study area, we systematically calculated the mass budget for all of the hillslope and channel processes present in these catchments. We identified the mass of sediment transported by each processes using a combination of multi-temporal mapping using high resolution satellite imagery or from values reported in the literature, each calculation is described in detail below. We assume that minimal sediment was present in the landscape prior to the earthquake, an observation supported by the observations of narrow channels and large areas of exposed bedrock in pre-earthquake images. The primary source of post-earthquake sediment are co-seismic mass movements (landslides and debris flows) and minor post-seismic mass movements. Debris flows are identified in the satellite imagery by their characteristic long and thin shape sometimes with visible levees, while landslides are wide with no channelization visible (Figure 2).

Sediment generated on hillslopes can either be stored on the hillslope or transferred into and stored in the tributary channels or Min Jiang. There are many processes that contribute to the transfer of sediment within the tributary catchments (Figure 2). Coseismic landslide debris can be eroded by overland flow which we estimate based on observations in the literature scaled to the study area. Coseismic landslides can be eroded by subsequent mass movement processes that may, in some cases generate debris flows. We term the general processes of erosion by mass movement as remobilization and further designate this into channelized and unchannelised forms (Fan, Juang, et al., 2018). Channelized remobilisations are triggered within previous mass movement material and are long and thin and are likely to have created debris flows. Unchannelised remobilisations were polygons without any clear channelization and can be formed by shallow landsliding within a previous deposit or may be produced by a dense, impossible to resolve from the imagery, rill network (Figure 2b). We constrain the mass of landslides and unchannelised remobilisations using area-volume scaling relationships, however no consistent scaling relationship exists for debris flows. The volume of debris flows is calculated as the residual after constraining the volumes of all other processes in the mass balance calculation. Once material has been eroded from hillslopes, it can either be stored within the tributary catchments or enter the Min Jiang. We use changes in channel deposit width observed on the satellite imagery and assumptions about channel shape to estimate changes in channel storage within the tributary catchments.

A number of processes can transfer mass from tributary catchments into the Min Jiang. Numerous extremely large, catchment clearing, debris flows occurred during the monsoons of 2008, 2010, 2013, and 2019. These created fans in the Min Jiang whose volume was measured and published (Fan, Scaringi, Domènech, et al., 2019; Yang et al., 2021). Additionally fluvial processes can erode channel material, the bedload component of this can be estimated from changes in storage within the tributary channels, while suspended sediment loads have been estimated in the literature.

To compute our estimates of the total sediment budget of the 10 years following the Wenchuan earthquake we used a Monte Carlo simulation framework. This framework allowed us to constrain the considerable uncertainty

of each process and the final budget. For each of the epochs (2009–2011, 2012–2013, 2014–2015, 2016–2018 as defined by the availability of satellite imagery coverage) within our study period we ran 10,000 simulations within which we produced an estimate of the volume of sediment mobilised by each process by sampling from their uncertainty. We describe the processes and their uncertainty in detail in the section below.

2.3. Sediment Sources: Mass Movements

We constrained the volume and mass of sediment generated within each epoch of our study with a multi-temporal mass movement inventory. This inventory is an adapted version of the inventory described in (Fan, Scaringi, Domènech, et al., 2019), here we will briefly describe the methodology used to generate this inventory and key alterations.

The inventory is derived from orthorectified satellite (and some aerial) imagery of 6 different years after the earthquake (Table S1 in Supporting Information S1). The 2011 image provided coverage of the entire area in high resolution and hence was chosen as the geo-referencing base for the study. Each image was orthorectified using the Pix4D software before detailed checks were employed to ensure there were no major rectifying errors between the inventories (Williams et al., 2018). The timing of these images defines the epochs of our sediment budgets; 2008 (coseismic budget), 2009–2011, 2012–2013, 2014–2015, 2016–2018.

In each image Fan, Scaringi, Domènech, et al., 2019 visually mapped any new mass movements (mass movements originating in previously un-failed hillslope material) along with any remobilization within the mass movements mapped in a previous image. All mass movements were mapped as polygons which covered the entire area of the mass movement, no effort was made to separate the source and deposition areas. As the landslide polygons were mapped by hand, particular attention was taken to avoid the amalgamation of multiple landslides into a single landslide polygon. New mass movements were primarily identified via changes in vegetation and supported by identification of channels, rills, and movement of boulders. Rather than rely on the "activity level" used in the original inventory (defined by the area of a mapped landslide not covered by vegetation; Chenxiao Tang et al., 2016; Fan, Scaringi, Domènech, et al., 2019) we explicitly map the remobilized area as its own polygon allowing the construction of a sediment budget. These "remobilisations" were mapped by comparing different images and identifying changes within previously mapped mass movements regardless of vegetation cover (Figure 2, Figures S1 and S2 in Supporting Information S1). These changes could be the formation of rill networks, debris flows or landslide scars, or the clear movement of boulders. Any mass movement which intersected with a previously mapped mass movement was classified as a remobilization, as it likely entrained previously deposited sediment. Our mapping scheme allowed us to directly map the area of the remobilization which we then used as the base of our mass movement sediment budget.

Within this mapping scheme we classified four processes in each epoch; landslides, debris flows, unchannelised remobilisations, and channelized remobilisations using the definitions of Fan, Juang, et al. (2018) (Figure 2, Figure S2 in Supporting Information S1). This classification was determined visually based upon the shape of the mapped polygons. Debris flows polygons are long and thin possibly with visible levees while landslides are wide with no channelization visible (Hungr et al., 2014). We also classified the remobilization polygons using a similar scheme, however as less data exists for these processes, we used more generalised terms. Channelized remobilization polygons are triggered within previous mass movement material and are long and thin similar to debris flows. Unchannelised remobilisations were polygons without any clear channelization and can be formed by shallow landsliding within a previous deposit or may be produced by a dense rill network which are impossible to resolve from the imagery (Figure 2b, Figure S2 in Supporting Information S1).

The mapped surface area of a landslide is converted into an estimate of deposit volume using an empirical area – volume scaling relationship ($V = \alpha A^{\gamma}$ where V is the volume of the landslide, A is its scar area and α and Y are empirical parameters). This methodology of estimating landslide deposit volume is strongly impacted by how the surface area of the landslide is mapped. Ideally only the scar area of the landslide would be mapped as the runout zone of the landslide can significantly increase the surface area of the landslide without having a major impact on the resulting volume. If a mapped landslide polygon contains the runout zone of the landslide a correction must be applied, otherwise the resulting volume will be an overestimate. To avoid any overestimations resulting from mapping both landslide scars and runout we estimated the scar areas of our mapped landslides using the correction methodology developed by (Marc et al., 2018, 2019). This correction assumes the scar area is elliptical and

Table 1
The Results of the Monte Carlo Simulations

Reference	$Log_{10}\alpha$	Y	Total coseismic volume (km^3)	Total runout-corrected coseismic volume (km^3)	Total post-seismic volume (km^3)	Total runout-corrected post-seismic volume (km^3)
(Larsen et al., 2010) Global landslides	−0.836 ± 0.015	1.332 ± 0.005	0.6 (±0.001)	0.2 (±0.0004)	0.003 (±0.00003)	0.0007 (±0.00001)
(Larsen et al., 2010) Global bedrock landslides	−0.73 ± 0.06	1.35 ± 0.01	1 (±0.001)	0.2 (±0.002)	0.004 (±0.0001)	0.001 (±0.00003)
(Larsen et al., 2010) Mixed Himalayan landslides	−0.59 ± 0.03	1.36 ± 0.01	1 (±0.007)	0.4 (±0.002)	0.007 (±0.0001)	0.001 (±0.00003)
(Guzzetti et al., 2009) Global landslides	−1.131	1.45 ± 0.009	1 (±0.004)	0.3 (±0.001)	0.004 (±0.00007)	0.0009 (±0.00002)
(Parker et al., 2011) Longmenshan landslides	−0.974 ± 0.366	1.388 ± 0.087	2 (±0.1)	0.4 (±0.04)	0.006 (±0.002)	0.001 (±0.0004)
(G. Li et al., 2014) Longmenshan landslides	−0.995 ± 0.366	1.392 ± 0.087	2 (±0.1)	0.4 (±0.04)	0.006 (±0.002)	0.001 (±0.0004)
Combined			1 (−0.6/+0.5)	0.3 (±0.1)	0.005 (±0.002)	0.001 (±0.0005)

Note. Each set of parameters is run 10,000 times and combined to produce an overall estimate of total volume and uncertainty. Coseismic volume includes all landslides that are mapped in the 2008 image while the post-seismic volume includes all new landslides mapped after this year. No other process was included. Total corrected volumes refers to the area derived from the scar area correction derived by (Marc et al., 2018).

uses an estimated ellipse aspect ratio, derived from the area and perimeter of the mass movement, to determine the area of the scar. Prior to applying this correction, we checked each landslide and remapped any which had amalgamated multiple landslides into a single polygon. Amalgamation can cause surface area overestimation (Marc & Hovius, 2015). We apply the scar area correction to all landslides and unchannelised remobilisations in our inventory. To determine the impact of this correction on estimations of landsliding volume we calculate the total volume for both the corrected and non-corrected volumes.

In our field location, the area – volume scaling parameters are uncertain as only a small number of landslides have had their volumes recorded. Many global and some local scaling parameters have been published but there is significant variation between the estimated parameter values (Larsen et al., 2010; G. Li et al., 2014). In order to constrain the impact this uncertainty has on estimating the volume of sediment generated by landslides we estimated the total landsliding volume using the Monte Carlo simulation methodology proposed by Li et al. (2014). Within each of our sediment budget Monte Carlo runs we randomly sampled from each of six sets of scaling parameters (Table 1) to generate an estimate of the total landsliding volume for that epoch. For each simulation we randomly choose six α and Y values for each polygon (1 for each scaling parameter set) by assuming a uniform distribution within the uncertainty stated in Table 1. We then summed the total landsliding volume estimated by each scaling parameter set and reported the median volume across these values for use in that budget simulation run. Finally, we then calculated the median and standard deviation of all 10,000 simulations to determine the uncertainty of the total landsliding volume.

2.4. Sediment Transfer and Temporary Storage – Tributary Channel Deposits

We mapped the width of the channel deposits on average every 200m along the tributary channels, from the head of the tributary to its confluence with the Min Jiang for the 17 largest catchments in our study area. For each epoch the resolution of the satellite imagery was 2.5 m and the length of time between catchment surveys varied from 1 to 3 years. The width of the channel deposit was defined as the length of a straight line from one edge of the non-vegetated sediment bed of a channel to the other (Figure S3 in Supporting Information S1). Each cross section was mapped in section of the valley free from landslide deposits which impinged directly onto the drainage network so that only sediment within the channel bed was included in the survey.

To convert the mapped widths into volumes we assumed the cross sectional area of the channel was either rectangular, trapezoidal or a circular segment (Figure S4 in Supporting Information S1). Varying between the volume estimates produced by using these shapes in each Monte Carlo run provides an estimate of uncertainty. For each cross sectional area we estimated the depth of the tributary channel deposits from the mapped widths using an empirical relationship derived by (Moody & Troutman, 2002). This scaling relationship is based upon thousands of river cross sections taken across several orders of magnitude of drainage area. Here we assume each valley was shaped by fluvial processes and subsequential filled with sediment. Each depth derived from the mapped width

of the channel deposits is therefore a maximum depth to the bedrock bottom of the channel. To calculate the area of trapezoid cross sections we also required an estimate of the bank angle of the tributary catchment. Within a buffer of 100 m from the mapped widths, the bank angles varied between 25 and 35°. We varied the bank angle between this range 10,000 times for each width and calculated the mean area. The volume of the channel material was calculated by integrating across the distances between the surveys.

Changes in the volume stored within channels were measured via changes in the mapped channel widths between epochs. If the width expanded we assumed there had been a depositional episode and so subtracted the previous estimate of stored sediment from the new larger volume to determine the increase in storage. If the width had not changed between the epochs we assumed that no deposition had occurred. Instead, we mapped the width of the active channel which was incising through the channel deposits, and estimated the volume of sediment mobilised by this incision, and assumed that it directly enters the Min Jiang. The mapped active channel (identified by the presence of water) is likely a result of debris flow activity and fluvial reworking of the sediment and therefore this process is termed incision within our sediment budget.

As the 17 catchments were not surveyed at the same time the number of surveys and the time between each survey differs for each catchment. Therefore, to determine a sediment budget across the epochs of the mass movement sediment budget for the entire study area, we averaged the sediment budget of each catchment. For each epoch of the catchment surveys we divided the change in sediment storage by the time between the surveys (units of m^3/yr.). This averaged rate was then combined with the results of the rest of the catchments to produce an average change in storage estimate for the entire area. Finally, we multiplied the average rate by the number of surveyed catchments (units of m^3) and across each epoch to allow us to compare the 2 sediment budgets.

Our uncertainty in cross sectional shape can cause tributary channel deposit volume to vary by up to 3x and up to 6x in our incision removal estimates. This variation is likely to be more significant than that of the lack of a true width-depth ratio for the deposits. If the valleys are primarily shaped by debris flows rather than fluvial processes, they are likely to be deeper with steeper sides than fluvial channels (Frank et al., 2015). The covariance in shape and depth resulting from different formation processes suggests that our methodology of considering multiple channel shapes should account for any uncertainty resulting from using a fluvial width – depth scaling.

2.5. Sediment Transfer – Remobilisations and Debris Flows

To link the mass movement and channel width sediment budgets together we needed to calculate how much sediment was being mobilised from the hillslopes in each epoch. We did this through estimating the volumes of the remobilization polygons and estimating how much of this entered into the channel network.

The area-volume scaling relationship for remobilization processes is poorly constrained, particularly for the channelized processes. For unchannelised remobilisations we used the same area – volume scaling methodology used for landslides as described in Section 2.3. However unlike coseismic landslides which can originate in bedrock, the volume of a remobilization is limited by the depth of the deposit it originates in. Therefore, if a particular combination of area-volume scaling parameters produced a depth of remobilization greater than the depth of the landslide deposit it originated in the chosen parameters were discarded and the scaling parameters were redrawn. This threshold ensures the volume of sediment of the unchannelised remobilisations is constrained by the volume of sediment available in the individual hillslope deposits. We also included an extra set of landslide area – volume parameters for the unchannelised remobilisations, the shallow landsliding parameters determined by Larsen et al. (2010) ($\mathrm{Log}_{10}\alpha = -0.836 \pm 0.015$, $Y = 1.145 \pm 0.008$). This set of parameters encourages the Monte Carlo simulation to produce shallower depths for the remobilisations compared to the new landslides on unfailed hillslopes.

The volumes of debris flows and channelized remobilisations are harder to quantify as flowing mass movements gain volume through entrainment of loose sediment along their runout path. While some estimates of the volume of sediment entrained by debris flows do exist (Ma et al., 2017; Santi & Morandi, 2013) these are empirical and poorly constrained. Further, in order to ensure our sediment budgets are balanced we calculate the volume of the debris flows and channelized remobilisations by comparing the change in the volume of sediment stored in the tributary channel deposits with the volume of sediment leaving the hillslope. The residual of this comparison is assumed to be due to debris flows and channelized remobilisations entering the tributary channel deposits. As

the volume of sediment mobilised by debris flows cannot be negative, the Monte Carlo simulation was rerun if a negative value was generated.

To determine the volume of sediment entering the tributary channel deposits or Min Jiang from remobilisations we defined a hillslope/channel drainage area threshold. If the maximum drainage area of an unchannelised remobilization polygon was greater than the threshold, the calculated volume of the polygon was assigned to the channel network. The threshold was derived from a threshold based channel extraction algorithm in the software LSDTopoTools (Mudd et al., 2020). An initial estimate of a threshold was derived from mapping likely channel head locations in satellite imagery. However, due to the uncertainty in this approach we produced a second threshold from the LSDTopoTools generated channel network. This final threshold was derived from the median drainage area of the first order channels (700,000 m^2). If a remobilization shapefile had a drainage area greater than this threshold it was assigned to the tributary channel deposits. Any polygon which had a maximum drainage area greater than that of a Strahler stream order 6 channel (the smallest order of the main trunk in the derived channel network) was automatically assigned to the Min Jiang rather than the tributary channel deposits, termed coseismic Min Jiang deposits or remobilized into the Min Jiang in our budget.

Within this budget we assume only remobilisations and debris flows can deposit sediment into tributary channel deposits. No undercutting of landslide deposits by the tributary channels was identified in either field observations or imagery, instead most landslides were remobilized by hillslope processes. We also do not see widespread rapid incision of deposits within the channel network (Croissant et al., 2017), this is likely due to the wide tributary channel floors isolating debris from the active channel. It is not common to see large landslides damming the tributary channels in our study area, although this is seen in many other locations within the earthquake impacted area (Fan et al., 2012) suggesting this form of erosion could be significant when the conditions are favorable. The tributary channels are small and do not have the transport capacity to mobilize the coarse sediment of the deposits. Therefore, in our sediment budget all landslides are initially added to the hillslope deposit store unless they are deposited directly into the Min Jiang. Debris flows by contrast can deposit directly into the tributary channel deposits (or the Min Jiang) as their greater mobility allows them to travel along the channel before depositing. To produce an estimate of sediment mobilised into the tributary channel deposits during the earthquake we applied the runout correction methodology to the coseismic debris flow polygons and added the resulting volumes to the tributary channel deposits. As we do not consider any potential sediment gained during the runout of the debris flow, our initial estimate of the volume within the tributary channel deposits is likely to be an underestimation.

2.6. Sediment Transfer – Overland Flow Erosion

The loose sediment on the hillslopes, particularly fine-grained sediment can be mobilised by runoff into the tributary channel deposits. This process occurs on small scales and is unlikely to be visible on satellite imagery. We estimated the volume of sediment mobilised by this process by scaling the field measurements performed by Fusun et al. (2013). They deployed sediment traps to record the volume of sediment leaving landslides over a single monsoon period. We extrapolated the reported erosion, assuming a constant rate, across the active bare area of the mass movements for each time step. We do not consider the impact the variability of rainfall may have on this process, thus our estimates are could be an overestimation considering the strong monsoon which occurred during the original study (Fusun et al., 2013; Shen et al., 2020). We also do not consider the impact topography, slope or drainage area, may have on overland flow. However as the erosion rates of this process are 2 orders of magnitude lower than the major erosional processes, we would not expect these parameters to have a significant effect on the overall budget. The uncertainty reported in our mass balance is as reported in the source material (±107.39 g of sediment per meter squared of unvegetated sediment per year).

2.7. Sediment Export – Catchment Clearing Debris Flows

Catchment clearing debris flows are large debris flows which evacuate sediment from the hillslopes and tributary channels and deposit it directly into the Min Jiang (Figure 2e). These debris flows produce large depositional fans which intersect directly with the main trunk of the Min Jiang. A database of the volumes of these depositional fans was compiled from technical reports and papers by (Fan, Scaringi, Domènech, et al., 2019). As uncertainty data was unavailable for most of the events, we assumed an uncertainty of ±50% of the reported volume. Catchment clearing debris flows mobilize sediment from both the hillslope and tributary channel deposits. They can be

triggered by landsliding on the hillslopes, run off within the channel, or the merging of multiple smaller debris flows (P. Cui et al., 2013; C. Tang et al., 2012). Debris flows can also bulk significantly along their runout with sediment from along the channel bed producing total deposit volumes at least an order of magnitude greater than their initiation volumes (Horton et al., 2019). As the majority of the sediment entrained by its runout is redeposited before the debris flow reaches the Min Jiang, we assume the recorded volumes of catchment clearing debris flows are equally made up of hillslope and tributary channel deposits.

2.8. Sediment Export – Suspended Sediment

Suspended sediment is an indicator of fluvial export of sediment in a catchment area and thus we include it as a process within our budget. The suspended sediment load does not include bedload transport into the Min Jiang so we have attempted to estimate this separately (incision). We estimated the mass of coseismic sediment mobilised by this process using the records of sediment discharge of the Min Jiang and other rivers reported by Wang et al. (2015). Wang et al. (2015) compiled yearly records of suspended sediment discharge for a number of sampling stations on rivers draining the epicentral area of the earthquake. For each station they reported pre (2006–2007) and post (2008–2012) earthquake sediment discharges and the mass of the landslides upstream of the station. We used this data to determine a simple linear trend ($r^2 = 0.46$) between the mass of landsliding upstream of a station and the increase in yearly suspended sediment discharge. We used this trend to estimate the suspended sediment transport related to the earthquake in our area. As we do not have any data covering the study area beyond 2012, we simply assume that the suspended sediment discharge remains constant. This is likely to be an overestimation as many studies have indicated that suspended sediment discharge decreases to its background rate within a decade of the earthquake (Hovius et al., 2011; J. Wang et al., 2015; W. Wang et al., 2017). Uncertainty in our values is derived from the uncertainty within our coseismically generated sediment mass estimates (Table 1). We assumed all sediment mobilised by this process originated within the tributary channel deposits.

2.9. Calculating Sediment Mass Budgets

To calculate our two mass balances, hillslope and tributary channel deposits, we use a Monte Carlo approach whereby the volume of sediment mobilised by each process is determined by randomly sampling from their respective uncertainties. We have identified that the only major process that we do not have a constrained method for calculating the volume of is debris flows (both channelized remobilization and new debris flows). Therefore, we calculate their volume as the residual of the comparison between the volume of sediment entering the tributary channel deposits (constrained by the mass movement inventory) and the change in the volume of sediment stored in the tributary channel deposits (constrained by our channel width inventory). Therefore our complete budget is calculated as

$$\begin{aligned}\text{Debris flows (Channelised remobilisation + New debris flows)} = \text{Change in tributary channel deposits} + \text{Suspended sediment} + \text{Incision} + (0.5 \times \text{Catchment clearing debris flows}) - \text{Overland flow erosion} - \text{Unchannelised remobilisation} \quad (1)\end{aligned}$$

To convert the resulting sediment volume budgets into mass budgets we must multiply the volumes by a density. As the density of the sediment with our study (and how it may change between stores) is not known we use a further Monte Carlo simulation for the conversion. We randomly sample from the estimated range of volumes mobilised by each process and multiply this by a random density chosen from a suitable range. For the density we used an estimate typical of alluvial sediment 2000 (±300) kg/m^3. In the main text we present all of our results in terms of mass while in supplemental Tables 2 and 4 the results can be found in terms of volume.

3. Results

3.1. Full Post-Earthquake Sediment Budget

In the study area, we mapped a total of 15,130 mass movements (8,830 coseismic and 6,300 post-seismic) across the study period (Figure 1b). These mass movements generated a total volume of 0.3 (±0.1) km^3 of sediment which has an estimated mass of 530.8 (±279.2) Mega tonnes. 99% of the sediment was generated coseismically,

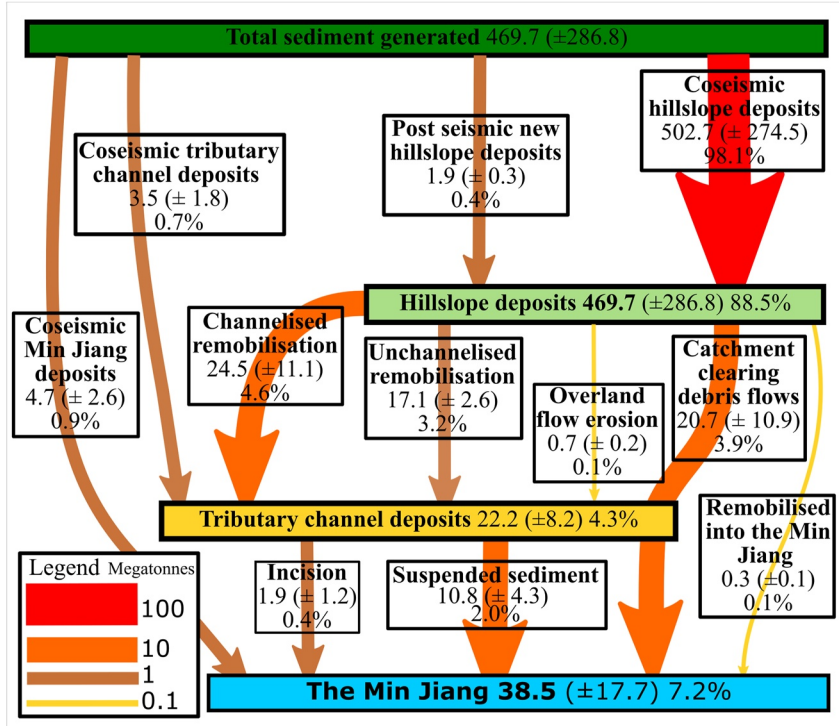

Figure 3. The sediment budget of the Wenchuan Earthquake. The width and color of each arrow indicates the magnitude of the sediment moved by the process between the stores. Each arrow is labeled with the process it represents with the median mass estimate. The uncertainty of each estimate is reported in brackets. We assume that catchment clearing debris flows begin on the hillslope and erode sediment from the tributary channel deposits before depositing the sediment into the Min Jiang without depositing sediment into the tributary channel deposits. Therefore we represent this as a single arrow passing through the tributary channel deposits and ending in the Min Jiang.

indicating any post-seismic enhancement of landsliding is not a significant contributor to post-seismic sediment discharges. Of the sediment that was mobilised from the hillslopes after the earthquake, less than 1% was from new post-seismic mass movements suggesting the increase in sediment discharge records is almost exclusively driven by remobilization of coseismic sediment. Only 12%, (4.7 Mt; ±2.6 Mt), of the sediment deposited into the Min Jiang was from coseismic landslide material deposited directly into the main trunk of the river (Table S2 in Supporting Information S1). The majority of sediment deposited into the Min Jiang after the earthquake travels through the tributary channels (Figure 3). Our observations demonstrate that the post-earthquake sediment cascade includes multiple steps within hillslopes and tributary channels prior to entering the Min Jiang.

At the end of the decade long study, 89% of the sediment generated during and after the earthquake remains on hillslopes. 4% is deposited in the tributary channels and the final 7% has entered the Min Jiang (Table S2 in Supporting Information S1). 99.6% of the sediment on the hillslope was generated during the earthquake. 80% (42.3 Mt; ±14.0) of the sediment remobilized from the hillslopes is deposited into the tributary channel deposits where it requires further remobilization before it is evacuated from the orogen.

The sediment mass mobilised by channelized remobilization peaks between 2012 and 2013 before declining sharply after 2015 (Figure 4). This is offset from peaks in the frequency of channelized remobilisations and new debris flows (Table S3 in Supporting Information S1) immediately after the earthquake. This discrepancy could reflect a change in the average size of the remobilisations or be due to an underestimation of the sediment entering the channel network un the first epoch. This underestimation could be due to a lack of imagery before 2008 to estimate the volume of sediment within the channel deposits prior to the earthquake. We estimate that channelized remobilisations mobilize 24.5 (±11.1) Mt of sediment after the earthquake, most of which enters the tributary channel deposits. These remobilisations are the most significant sediment remobilization process in the post-earthquake landscape.

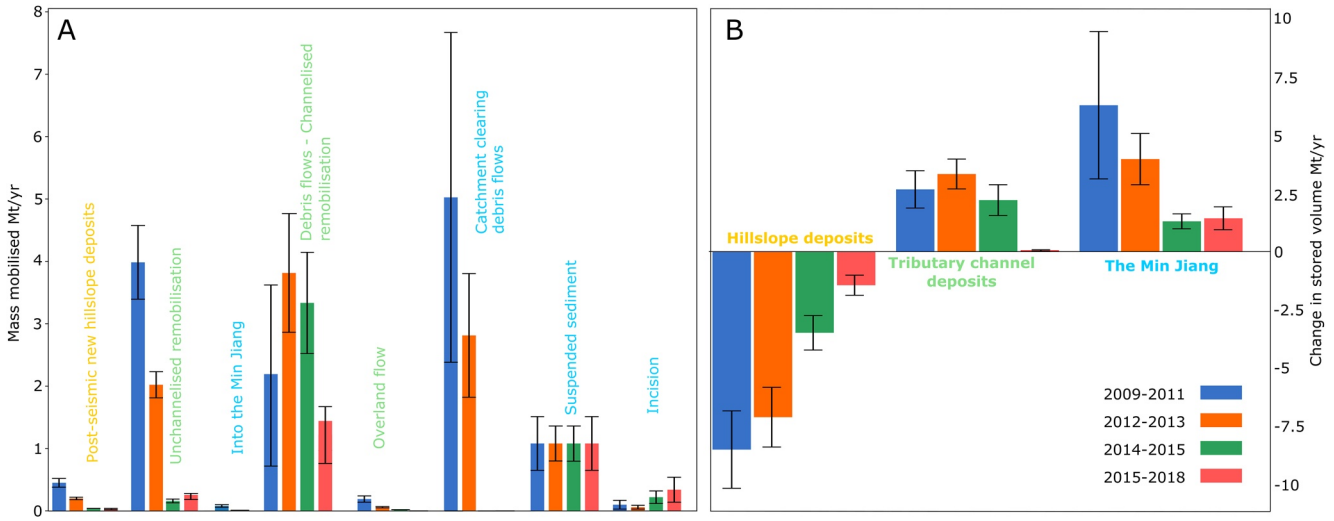

Figure 4. The sediment mass budget. (a) Each bar represents the average rate of sediment mobilised by a process during the given epoch. (b) Each bar represents the average rate of change of the mass of sediment stored during the given epoch. The rate at which the sediment stored changes is controlled by the balance of the processes depositing into the stores and those that erode from it. The names of the processes are colored by the store that they deposit in.

Large catchment clearing debris flows are the major process depositing sediment into the Min Jiang accounting for 61% (20.7; ±13.8 Mt) of the sediment deposited into the river after the earthquake. Debris flows (both small channelized remobilisations and large catchment clearing flows) dominate the sediment budget accounting for 67% (45.9; ±22.0 Mt) of all sediment mobilised after the earthquake. Fluvial processes (here represented by incision and suspended sediment), on the other hand, are only minor contributors to sediment transport over our study period.

3.2. The Sediment Budget Through Time

Separating the budget into 4 post-earthquake epochs (2009–2011, 2012–2013, 2014–2015, and 2016–2018 inclusively) defined by the availability of satellite imagery allows us to analyze how the processes and overall discharge changes through time. We find that the total mass of sediment mobilised each year decreased by an order of magnitude from 12.6 (±5.2) – 2.9 (±1.1) Mt/yr. between 2011 and 2018 (Figure 4, Table S4 in Supporting Information S1). A total of 77.9 (±30.0) Mt of sediment (both new and remobilized coseismically generated) is mobilised after the earthquake, 76% of which was mobilised during the first 5 years after the earthquake. The total sediment discharge decreases rapidly until 2015 after which it begins to level off suggesting it had begun to stabilize by the end of the study period.

The rate at which the hillslope deposits are depleted decreases from 8.5 (±1.7) Mt/yr.–1.4 (±0.4) Mt/yr. over our study period. For each epoch the volume of sediment produced by post-seismic mass movements (new landsliding) is less than the volume remobilized from the hillslope deposits. This decrease in remobilization rates coincides with the overall decrease in sediment discharge. As remobilization of coseismic deposits continues to dominate the hillslope sediment discharge at the end of our study period, it is likely the overall discharge remains elevated above pre-earthquake levels.

Tributary channels have aggraded across the study period. The change in storage of the tributary channel deposits declines sharply after 2015 but still remains slightly positive (Figure 4). The major cause of the decrease in the tributary channel deposit budget seems to be due to a decrease in the rate of sediment being deposited into the channels. A slight increase in the mass of sediment leaving the deposits via incision is observed, but is well within the uncertainty of our budget. If the deposition of sediment into the tributary channel deposits remains low it is likely the total volume of sediment stored will begin to decrease in the future.

Finally, we see an overall decrease in the sediment mass entering the Min Jiang across the study period. This coincides with changes in the frequency of large catchment clearing debris flows. Without these large flows the volume of sediment entering the Min Jiang decreases by almost a factor of 6, highlighting the importance of the largest mass movement events to evacuating the coseismic sediment from the Longmen Shan.

4. Discussion

Our full sediment budget of the Wenchuan earthquake reveals that more than 88% of the sediment produced by the earthquake remains on hillslopes 10 years after the earthquake. The majority of the coseismically generated sediment is mobilised by channelized remobilisations (which we interpret to be debris flows) which deposit sediment to the base of the hillslopes or rare large catchment clearing flows which can bypass the tributary channel deposits and mobilize sediment directly into the Min Jiang. Throughout geological history the frequency of events on the scale of the largest catchment clearing debris flows is significantly lower than what we see after the earthquake (Korup, 2012). Therefore, the high frequency of catchment clearing debris flows we have observed is unlikely to be sustainable for the long term and a decrease should be expected. Without these large catchment clearing debris flows most sediment will be stored and transported multiple times before it is evacuated from the mountain range. This pattern of remobilization and deposition could be repeated multiple times likely extending the residence time of some sediment up to 100s if not 1000s of years.

As the residence time of sediment is strongly affected by the largest and rarest of events it is important to observe the area of interest for the longest time possible. For example, within our study area there were no catchment clearing debris flows between 2013 and 2018 which dramatically decreases the sediment erosion rate of the area which would decrease any estimates of residence time. However, in August 2019 a large storm (maximum intensity 28.5 mm/hr) triggered 12 large catchment-clearing debris flows in our study area, some in catchments where no debris flow had occurred for over 5 years (Fan et al., 2020; Yang et al., 2021). Initial estimates of the volume of the debris flows suggested a total of 1.9×10^{-2} ($\pm 3 \times 10^{-2}$) km^3 of sediment was transported by these events (Yang et al., 2021). Field investigation of the debris flow deposits revealed that the majority of the sediment was deposited within the tributary catchments, only a small volume was deposited into the Min Jiang. As a crude estimate of the volume of sediment deposited into the Min Jiang, we can extrapolate the recorded volume of a single debris flow fan over all of the 12 flows. The deposition fan of the Manianping catchment has an estimated volume of 7×10^{-4} km^3 (Yang et al., 2021) assuming all 12 flows were of equal magnitude, 8.4×10^{-3} km^3 of sediment was deposited into the Min Jiang. Assuming a deposit density of 2000 kg/m^3 we can estimate the impact of these flows upon our sediment budget. These flows potentially deposited 16.8 Mt of sediment into the Min Jiang almost doubling the final epoch's yearly average sediment mobilization rate. Interestingly many of the 2019 catchment clearing debris flows occurred without significant remobilization of hillslope deposits, indicating they only removed sediment from the tributary channel deposits (Fan et al., 2020). This could demonstrate a long-term shift in behavior as the stabilization of the hillslope deposits causes the tributary channel deposits to become the main sediment source in the epicentral area.

Our sediment budget, and the observations of others, reveals that the frequency of remobilization of hillslope deposits has decreased since the earthquake. In the first epoch (2009–2011) of our budget we recorded 4,296 remobilization events, 1,193 of which were channelized. However, in the final epoch (2016–2018) just 54 remobilisations were recorded (11 channelized; Table S3 in Supporting Information S1). This pattern is not mirrored in the mass transport rates of the remobilization processes (Figure 4). There is a rapid decline in the mass transport rate from 2011 to 2015 followed by a slight increase in the final epoch 2016–2018. This rise reflects changes in the magnitude of remobilized deposits despite a reduction in frequency. In the final epoch the mean scar area of an unchannelised remobilization was 3,600 m^2 (mean mass of 17 tonnes), while during the previous epoch (2014–2015) it was just 1540 m^2 (mean mass 5.7 tonnes). We interpret the uptick in mass transport rate across the final epoch to a stochastic effect due to the short lengths of our epochs. This is also true of channelized remobilisations. The volume of a debris flow deposit is a function of its initial failure volume and the volume of sediment it entrains during its runout (Horton et al., 2019; Richard M. Iverson et al., 2011). Therefore, any change in the mobilization rate of these mass movements is due to a change in either of these factors. Channelized remobilization mass transport rates initially increase between 2009 and 2013 before decreasing through to 2018. Channelized remobilisations occurred in larger coseismic landslide deposits in the 2012–2013 epoch (median area 17,000 m^2) than in the 2009–2011 epoch (median area 14,000 m^2) suggesting they had a greater potential to

entrain sediment, leading to a rise in mass transport rate. Channelized remobilisations occurred in larger deposits between in the 2014–2015 (median area 25 000 m^2), which may have helped to maintain higher mass transport rates, despite an order of magnitude decline in frequency (Table S3 in Supporting Information S1). The final epoch 2016–2018 saw a significant decrease in both the frequency of channelized remobizations and the area of co-seismic deposits that they were occurring in (median area 12,000 m^2). The combination of these two trends likely drives the 60% decrease in sediment mobilization rate.

The relationship between mass transport rates and frequencies of both unchannelised and channelized remobilisations is non-linear and complex. Hence the changing frequency of remobilization events must be considered with changes in the spatial patterns of the location and size of remobilization events. Fan, Domènech, et al., 2018 showed how through time the frequency magnitude of the landslides being remobilized changed, with larger landslides more likely to remain active for longer. Fan et al., 2020 demonstrated that post seismic landslides were more likely to occur on hillslopes with large volumes of coseismic landslide sediment deposited onto them than form on unfailed hillslopes for the majority of the first decade after the Wenchuan earthquake. These trends highlight that the vast amount of landslide deposits, many of which are small, stabilize within the first 10 years after the earthquake. This stabilization drives the decrease in mass transport rates rather than exhaustion of available sediment. This apparent stabilization of hillslope deposits will extend the residence time of co-seismically generated sediment beyond that of what can be expected from rates recorded here. The reduction in debris-flow frequency we observe is also reported in other studies and after other earthquakes; rainfall intensity duration thresholds in the epicentral area have increased since the earthquake leading to indications of a stabilization of the coseismically generated sediment taking place (Dahlquist & West, 2019; Fan et al., 2020; S. Zhang & Zhang, 2017).

The mechanisms causing the stabilization of co-seismic mass movements are not well understood through time, however there are several hypotheses which we will discuss here. The first is that colonization of the landslide area by vegetation has increased the resistive strength of the landslide deposit. Vegetation can stabilize the deposit in several ways. The canopy of vegetation can intercept the rainfall before it strikes the sediment reducing the local intensity and saturation state (McGuire et al., 2016; Wilkinson et al., 2002). While the trunks and stems of vegetation increase the roughness of the slope reducing the velocity of surface runoff and reducing shear stress of any overland flow. Vegetation can also increase the shear strength of the soil (T. C. Hales et al., 2009; Tristram C. Hales, 2018). A correlation between NDVI (Normalised Difference Vegetation Index) and the reduction in remobilization frequency have suggested that vegetation regrowth may be the mechanism by which this deposits stabilize (Fan, Domènech, et al., 2018; Yunus et al., 2020). However the first type of vegetation to colonize landslide areas are grasses and shrubs (Shen et al., 2020), most of which only have shallow and weak root structures which do not add significant strength to the sediment (Tristram C. Hales, 2018). The impact of vegetation may depend on triggering mechanism, as it is unlikely that grasses will have a large impact on debris flows and channelized remobilization triggered by shallow landsliding, but may impact surface runoff. While it is clear that there are many mechanisms by which sediment can be stabilized by vegetation, it is unlikely that vegetation is solely responsible for the trends that we see after the earthquake.

Another stabilization mechanism is internal erosion of the hillslope deposits (Peng Cui et al., 2014; W. Hu et al., 2016; Wei Hu et al., 2017; S. Zhang & Zhang, 2017). It is hypothesized that fresh landslide deposits are highly permeable allowing water to pass through the loose sediment with ease. As the water passes through the deposit it can entrain fine sediment and move it through the deposit. As the fine sediment moves through the deposit it can induce small localized failures by blocking small pore spaces and increasing pore pressures (Peng Cui et al., 2014). These small failures can coalesce to destabilize the deposit and cause a larger remobilization of the sediment. If there is enough fluid within the failing deposit a debris flow can be formed. However, if no large-scale failure occurs many sections of the deposit will be in a fines depleted state. These fines depleted areas will be more stable as they are more permeable resulting in a greater hydraulic conductivity and possibly a greater internal friction angle (W. Hu et al., 2016; Wei Hu et al., 2017). The smaller failures may also compact the deposits which can also reduce the likelihood of failure in loose sediment (Chang et al., 2011; R. M. Iverson et al., 2000). However, there is minimal in situ evidence for preferential erosion of fine sediment in coseismic landslide deposits.

Human activity may also have impacted sediment discharge due to engineering work within the channels (Fan, Juang, et al., 2018). This has the potential to significantly reduce the number of catchment-clearing debris flows

in the area. However as the population density of the epicentral area is low for the most part, only a small fraction of the hillslopes has been stabilized by engineering. Therefore, while the frequency of channel clearing debris flows could be influenced by human activity, the decrease in the mass transport rates from the hillslope cannot.

Finally, we need to consider the stochastic nature of mass movements. Mass movements are driven by stochastic rainfall events. Across our decadal observation window, we need to consider whether declines in mass-movement frequency are related to fewer triggering storm events. In the 10 years since the earthquake the most intense storm (1-hr intensity) occurred in 2013 (64.5 mm) with the second most intense occurring in 2017 (40.1 mm) (Shen et al., 2020). 2013 also experienced a similar amount of total precipitation to the 2011 but considerably less activity was recorded in 2013 across all scales (Fan, Scaringi, Domènech, et al., 2019; Fan, Scaringi, Korup, et al., 2019; F. Zhang et al., 2019). While the intensity of the monsoons vary year on year the frequency of observed sediment transport continually decreases (Table S3 in Supporting Information S1). There is no correlation between precipitation and mass movement frequency (or mass mobilization rate) following the earthquake.

The mass balance of first 10 years after the earthquake is dominated by mass movement events. Between 2013 and 2018 there are no catchment clearing debris flows and deposition into the Min Jiang more than halves (Figure 4). In contrast the fluvial driven processes (termed incision in our budget) are more consistent in the rate of sediment export to the Min Jiang, but the rate is much smaller. Incision only accounts for 5% of the sediment entering the Min Jiang during the first decade after the earthquake. Further, fluvial erosion is only observed acting on sediment that had already been remobilized by a previous mass movement process, there is little evidence that the tributary channels can erode the landslide deposits directly. The conclusion is that hillslope processes and their rates act as a primary control on the magnitude and time scales of sediment evacuation from the orogen. Fluvial erosion is likely slow at removing sediment from the tributary channel deposits due to the coarse nature of the stored sediment and low fluvial discharges. The coarse nature of the tributary channel deposits indicates that currently much of the sediment requires debris flows, large floods or in situ break down of the boulders before it can be mobilised out of the orogen.

While we have few constraints on sediment transport in the main trunk of the Min Jiang, the Zipingpu reservoir offers some insight into the sediment dynamics of the entire system. The Zipingpu reservoir is a man-made reservoir a few kilometres downstream of our study area. A borehole drilled in the center of the reservoir by (F. Zhang et al., 2019) in 2016 identified that the earthquake has only had a slight impact on the sediment dynamics of the reservoir. No change in sedimentation rate was noticed, likely due to the distal location of the core relative to the mouth of the Min Jiang entering the reservoir, but a change in the chemistry and grain size was observed (F. Zhang et al., 2019). Grain size increased, and the Rb/Sr ratio decreased potentially revealing an influx of coarser fresh (unweathered) landslide derived sediment into the reservoir. Crucially while these signals were recognised immediately after the earthquake, the biggest response was observed after the 2010 monsoon when catchment clearing debris flows deposited large volumes of sediment into the main trunks of the rivers feeding the reservoir. This result agrees with our finding that debris flows are the major component in delivering sediment to the channel network. The borehole also suggests that the system is in a transport-limited state as the increase in grain size is well correlated to annual runoff rates indicating the need for large events to mobilize much of the sediment (F. Zhang et al., 2019).

Our results validate modeling that indicates coseismic sediment has long residence times (10's-1000's of years; Croissant et al., 2019; Francis et al., 2020; Yanites et al., 2010). Empirical and modeling studies suggest that the hillslopes will continue to be perturbed for at least another decade before returning to background levels (Chen et al., 2020; C. Li et al., 2020; Shen et al., 2020; Yunus et al., 2020). As this trend in declining activity is driven by stabilization rather than exhaustion it is likely the residence time of the coseismically generated sediment will be significantly longer. Large earthquakes such as the Wenchuan earthquake have a return period of 500–4,000 years and if coseismically generated sediment can remain being reworked for similar timescales it is likely erosion rates will be altered (Francis et al., 2020; G. Li et al., 2017). The large volumes of sediment on the steep hillslopes, will continue to be mobilised, albeit much slower than immediately after the earthquake. Erosion rates in the tributary channels and the Min Jiang are likely to be lowered if the bedload is not mobilised at rates significant enough to abrade the bed. Deposits of landslide derived sediment have been linked to knickpoints within the Longmen Shan indicating the region is prone to long periods of reduced erosion (Fan, Yunus, et al., 2019; Ouimet et al., 2007). If post-seismic reduction of erosion rates is frequent and wide spread, it is possible that the largest earthquakes may

have a positive impact on the long-term mass balance of the mountain range despite the huge amount of erosion they initiate (Francis et al., 2020).

5. Conclusions

Here we have quantified the sediment cascade of the 10 years following the 2008 Wenchuan earthquake. Using a multitemporal landslide inventory, channel width surveys and constrained area – volume scaling relationships we tracked the evolution of 530.8 Mt of sediment. Of this sediment just 7% was deposited into the Min Jiang, the major orogen draining river of the study area. ~89% of the sediment deposited onto the hillslopes during the earthquake remains waiting to be mobilised into the channel network. The key process in mobilizing coseismic sediment into the Min Jiang is debris flows (channelized remobilisations and catchment clearing debris flows). The largest of these can deposit huge volumes of sediment from the tributary channels, overcoming the otherwise low transport capacity of the channels in these catchments. These large flows are highly stochastic and can occur after breaks of many years. Determining the frequency and magnitude of these events is crucial to estimating the residence time of the coseismically generated sediment. Finally, as large volumes of coseismically generated sediment can remain within the orogen for extended periods of time, their impact should be considered when modeling the long-term evolution of tectonically active mountain ranges.

Conflict of Interest

The authors declare no conflicts of interest relevant to this study.

Data Availability Statement

The original mass movement inventories upon which this study is based have been published (Fan, Scaringi, Domènech, et al., 2019) and can be found at https://doi.org/10.5281/zenodo.1405489. The adapted mass movement inventories, the channel width inventories and the Python code used in this study can be found at (https://zenodo.org/record/5676154).

Acknowledgments
This work was funded by the Newton Fund, Natural Environmental Research Council, Economic and Social Research Council, and National Science Foundation for China grant, NE/N012240/1, the Funds for Creative Research Groups of China (Grant No. 41521002), and the Fund for International Cooperation (NSFC-RCUK_NERC), Resilience to Earthquake-induced landslide risk in China (Grant No. 41661134010). The authors would like to thank the team of mappers who helped put together the mass movement inventory on which this study was based. We would also like to thank A. Densmore and M. Singer for useful discussions which greatly enhanced this paper. We also would like to acknowledge the helpful comments of Maxwell Dahlquist, Joshua N. Jones and an anonymous reviewer on previous versions of our manuscript. We would also like to thank the editorial team of Amy East and associate editor Odin Marc for their guidance through the review process.

References

Bennett, G. L., Molnar, P., McArdell, B. W., & Burlando, P. (2014). A probabilistic sediment cascade model of sediment transfer in the Illgraben. *Water Resources Research*, *50*(2), 1225–1244. https://doi.org/10.1002/2013WR013806

Burchfiel, B. C., Royden, L. H., van der Hilst, R. D., Hager, B. H., Chen, Z., King, R. W., et al. (2008). A geological and geophysical context for the Wenchuan earthquake of 12 May 2008, Sichuan, People's Republic of China. *Geological Society of America Today*, *18*(7), 4–11. https://doi.org/10.1130/GSATG18A.1

Campforts, B., Shobe, C. M., Steer, P., Vanmaercke, M., Lague, D., & Braun, J. (2020). HyLands 1.0: A hybrid landscape evolution model to simulate the impact of landslides and landslide-derived sediment on landscape evolution. *Geoscientific Model Development*, *13*(9), 3863–3886. https://doi.org/10.5194/gmd-13-3863-2020

Chang, D. S., Zhang, L. M., Xu, Y., & Huang, R. (2011). Field testing of erodibility of two landslide dams triggered by the 12 May Wenchuan earthquake. *Landslides*, *8*(October 2009), 321–332. https://doi.org/10.1007/s10346-011-0256-x

Chen, M., Tang, C., Xiong, J., Shi, Q. Y., Li, N., Gong, L. F., et al. (2020). The long-term evolution of landslide activity near the epicentral area of the 2008 Wenchuan earthquake in China. *Geomorphology*, *367*, 107317. https://doi.org/10.1016/j.geomorph.2020.107317

Croissant, T., Lague, D., Steer, P., & Davy, P. (2017). Rapid post-seismic landslide evacuation boosted by dynamic river width. *Nature Geoscience*, *10*(9), 680–684. https://doi.org/10.1038/ngeo3005

Croissant, T., Steer, P., Lague, D., Davy, P., Jeandet, L., & Hilton, R. G. (2019). Seismic cycles, earthquakes, landslides and sediment fluxes: Linking tectonics to surface processes using a reduced-complexity model. *Geomorphology*, *339*, 87–103. https://doi.org/10.1016/j.geomorph.2019.04.017

Cui, P., Guo, C. X., Zhou, J. W., Hao, M. H., & Xu, F. G. (2014). The mechanisms behind shallow failures in slopes comprised of landslide deposits. *Engineering Geology*, *180*, 34–44. https://doi.org/10.1016/j.enggeo.2014.04.009

Cui, P., Zhou, G. G. D., Zhu, X. H., & Zhang, J. Q. (2013). Scale amplification of natural debris flows caused by cascading landslide dam failures. *Geomorphology*, *182*(August 2010), 173–189. https://doi.org/10.1016/j.geomorph.2012.11.009

Dadson, S. J., Hovius, N., Chen, H., Dade, W. B., Lin, J.-C., Hsu, M.-L., et al. (2004). Earthquake-triggered increase in sediment delivery from an active mountain belt. *Geology*, *32*(8), 733. https://doi.org/10.1130/G20639.1

Dahlquist, M. P., & West, A. J. (2019). Initiation and runout of post-seismic debris flows: Insights from the 2015 Gorkha earthquake. *Geophysical Research Letters*, *46*(16), 9658–9668. https://doi.org/10.1029/2019GL083548

Dahlquist, M. P., West, A. J., & Li, G. (2018). Landslide-driven drainage divide migration. *Geology*, *46*(5), 403–406. https://doi.org/10.1130/G39916.1

Dai, F. C., Xu, C., Yao, X., Xu, L., Tu, X. B., & Gong, Q. M. (2011). Spatial distribution of landslides triggered by the 2008 Ms 8.0 Wenchuan earthquake, China. *Journal of Asian Earth Sciences*, *40*(4), 883–895. https://doi.org/10.1016/j.jseaes.2010.04.010

Densmore, A. L., Ellis, M. A., Li, Y., Zhou, R., Hancock, G. S., & Richardson, N. (2007). Active tectonics of the Beichuan and Pengguan faults at the eastern margin of the Tibetan Plateau. *Tectonics*, *26*(4), 1–17. https://doi.org/10.1029/2006TC001987

Densmore, A. L., Li, Y., Richardson, N. J., Zhou, R., Ellis, M., & Zhang, Y. (2010). The role of late quaternary upper-crustal faults in the 12 may 2008 Wenchuan earthquake. *Bulletin of the Seismological Society of America*, *100*(5 B), 2700–2712. https://doi.org/10.1785/0120090294

Densmore, A. L., Parker, R. N., Rosser, N. J., De Michele, M., Yong, L., Runqiu, H., et al. (2012). Reply to "Isostasy can't be ignored". *Nature Geoscience*, *5*(2), 83–84. https://doi.org/10.1038/ngeo1385

Dietrich, W. E., Dunne, T., Humphrey, N. F., & Reid, L. M. (1982). Construction of sediment budgets for drainage basins. *Workshop on Sediment Budgets and Routing in Forested Drainage Basins: SAVE Proceedings*, *31*, 5–23.

Egholm, D. L., Knudsen, M. F., & Sandiford, M. (2013). Lifespan of mountain ranges scaled by feedbacks between landsliding and erosion by rivers. *Nature*, *498*(7455), 475–478. https://doi.org/10.1038/nature12218

Fan, X., Domènech, G., Scaringi, G., Huang, R., Xu, Q., Hales, T. C., et al. (2018). Spatio-temporal evolution of mass wasting after the 2008 Mw 7 . 9 Wenchuan Earthquake revealed by a detailed multi-temporal inventory. *Landslides*, *15*(September), 2325–2341. https://doi.org/10.1007/s10346-018-1054-5

Fan, X., Juang, C. H., Wasowski, J., Huang, R., Xu, Q., Scaringi, G., et al. (2018). What we have learned from the 2008 Wenchuan earthquake and its aftermath: A decade of research and challenges. *Engineering Geology*, *241*(May), 25–32. https://doi.org/10.1016/j.enggeo.2018.05.004

Fan, X., Scaringi, G., Domènech, G., Yang, F., Guo, X., Dai, L., et al. (2019). Two multi-temporal datasets that track the enhanced landsliding after the 2008 Wenchuan earthquake. *Earth System Science Data*, *11*(1), 35–55. https://doi.org/10.5194/essd-11-35-2019

Fan, X., Scaringi, G., Korup, O., West, A. J., van Westen, C. J., Tanyas, H., et al. (2019). Earthquake-induced chains of geologic hazards: Patterns, mechanisms, and impacts. *Reviews of Geophysics*. *57*(2), 421–503. https://doi.org/10.1029/2018RG000626

Fan, X., van Westen, C. J., Korup, O., Gorum, T., Xu, Q., Dai, F., et al. (2012). Transient water and sediment storage of the decaying landslide dams induced by the 2008 Wenchuan earthquake, China. *Geomorphology*, *171–172*, 58–68. https://doi.org/10.1016/j.geomorph.2012.05.003

Fan, X., Yunus, A. P., Jansen, J. D., Dai, L., Strom, A., & Xu, Q. (2019). Comment on "Gigantic rockslides induced by fluvial incision in the Diexi area along the eastern margin of the Tibetan Plateau" by Zhao et al. *Geomorphology*, *338*, 27–42. https://doi.org/10.1016/j.geomorph.2019.106963

Fan, X., Yunus, A. P., Scaringi, G., Catani, F., Subramanian, S. S., Xu, Q., & Huang, R. (2020). Rapidly evolving controls of landslides after a strong earthquake and implications for hazard assessments. *Geophysical Research Letters*, *48*(1), e2020GL090509. https://doi.org/10.1029/2020GL090509

Francis, O. R., Hales, T. C., Hobley, D. E. J., Fan, X., Horton, A. J., Scaringi, G., & Huang, R. (2020). The impact of earthquakes on orogen-scale exhumation. *Earth Surface Dynamics*, *8*(3), 579–593. https://doi.org/10.5194/esurf-8-579-2020

Frank, F., McArdell, B. W., Huggel, C., & Vieli, A. (2015). The importance of entrainment and bulking on debris flow runout modeling: Examples from the Swiss Alps. *Natural Hazards and Earth System Sciences*, *15*(11), 2569–2583. https://doi.org/10.5194/nhess-15-2569-2015

Fusun, S., Jinniu, W., Tao, L., Yan, W., Haixia, G., & Ning, W. (2013). Effects of different types of vegetation recovery on runoff and soil erosion on a Wenchuan earthquake-triggered landslide, China. *Journal of Soil and Water Conservation*, *68*(2), 138–145. https://doi.org/10.2489/jswc.68.2.138

Gallen, S. F., Clark, M. K., & Godt, J. W. (2015). Coseismic landslides reveal near-surface rock strength in a highrelief, tectonically active setting. *Geology*, *43*(1), 11–14. https://doi.org/10.1130/G36080.1

Godard, V., Lavé, J., Carcaillet, J., Cattin, R., Bourlès, D., & Zhu, J. (2010). Spatial distribution of denudation in Eastern Tibet and regressive erosion of plateau margins. *Tectonophysics*, *491*(1–4), 253–274. https://doi.org/10.1016/j.tecto.2009.10.026

Guo, X., Cui, P., Li, Y., Ma, L., Ge, Y., & Mahoney, W. B. (2016). Intensity-duration threshold of rainfall-triggered debris flows in the Wenchuan Earthquake affected area, China. *Geomorphology*, *253*, 208–216. https://doi.org/10.1016/j.geomorph.2015.10.009

Guzzetti, F., Ardizzone, F., Cardinali, M., Rossi, M., & Valigi, D. (2009). Landslide volumes and landslide mobilization rates in Umbria, central Italy. *Earth and Planetary Science Letters*, *279*(3–4), 222–229. https://doi.org/10.1016/j.epsl.2009.01.005

Hales, T. C. (2018). Modelling biome-scale root reinforcement and slope stability. *Earth Surface Processes and Landforms*, *43*(10), 2157–2166. https://doi.org/10.1002/esp.4381

Hales, T. C., Ford, C. R., Hwang, T., Vose, J. M., & Band, L. E. (2009). Topographic and ecologic controls on root reinforcement. *Journal of Geophysical Research: Solid Earth*, *114*(3), 1–17. https://doi.org/10.1029/2008JF001168

Hinderer, M. (2012). From gullies to mountain belts: A review of sediment budgets at various scales. *Sedimentary Geology*, *280*, 21–59. https://doi.org/10.1016/j.sedgeo.2012.03.009

Horton, A. J., Hales, T. C., Ouyang, C., & Fan, X. (2019). Identifying post-earthquake debris flow hazard using Massflow. *Engineering Geology*, *258*, 105134. https://doi.org/10.1016/j.enggeo.2019.05.011

Hovius, N., Meunier, P., Lin, C. W., Chen, H., Chen, Y. G., Dadson, S., et al. (2011). Prolonged seismically induced erosion and the mass balance of a large earthquake. *Earth and Planetary Science Letters*, *304*(3–4), 347–355. https://doi.org/10.1016/j.epsl.2011.02.005

Hovius, N., Stark, C. P., Hao-Tsu, C., & Jiun-Chuan, L. (2000). Supply and removal of sediment in a landslide-dominated mountain belt: Central range, Taiwan. *The Journal of Geology*, *108*(1), 73–89. https://doi.org/10.1086/314387

Hu, W., Dong, X. J., Xu, Q., Wang, G. H., van Asch, T. W. J., & Hicher, P. Y. (2016). Initiation processes for run-off generated debris flows in the Wenchuan earthquake area of China. *Geomorphology*, *253*, 468–477. https://doi.org/10.1016/j.geomorph.2015.10.024

Hu, W., Scaringi, G., Xu, Q., Pei, Z., Van Asch, T. W. J., & Hicher, P. Y. (2017). Sensitivity of the initiation and runout of flowslides in loose granular deposits to the content of small particles: An insight from flume tests. *Engineering Geology*, *231*(July), 34–44. https://doi.org/10.1016/j.enggeo.2017.10.001

Huang, R., & Fan, X. (2013). The landslide story. *Nature Geoscience*, *6*(5), 325–326. https://doi.org/10.1038/ngeo1806

Hubbard, J., & Shaw, J. H. (2009). Uplift of the longmen Shan and Tibetan plateau, and the 2008 Wenchuan (M = 7.9) earthquake. *Nature*, *458*(7235), 194–197. https://doi.org/10.1038/nature07837

Hungr, O., Leroueil, S., & Picarelli, L. (2014). The Varnes classification of landslide types, an update. *Landslides*, *11*(2), 167–194. https://doi.org/10.1007/s10346-013-0436-y

Iverson, R. M., Reid, M. E., Iverson, N. R., LaHusen, R. G., Logan, M., Mann, J. E., & Brien, D. L. (2000). Acute sensitivity of landslide rates to initial soil porosity. *Science*, *290*(5491), 513–516. https://doi.org/10.1126/science.290.5491.513

Iverson, R. M., Reid, M. E., Logan, M., LaHusen, R. G., Godt, J. W., & Griswold, J. P. (2011). Positive feedback and momentum growth during debris-flow entrainment of wet bed sediment. *Nature Geoscience*, *4*(2), 116–121. https://doi.org/10.1038/ngeo1040

Keefer, D. K. (2002). Investigating landslides caused by earthquakes - a historical review. *Surveys in Geophysics*, *23*(6), 473–510. https://doi.org/10.1023/A:1021274710840

Kincey, M. E., Rosser, N. J., Robinson, T. R., Densmore, A. L., Shrestha, R., Pujara, D. S., et al. (2021). Evolution of coseismic and post-seismic landsliding after the 2015 M w 7.8 Gorkha earthquake, Nepal. *Journal of Geophysical Research: Earth Surface*, *126*(3), e2020JF005803. https://doi.org/10.1029/2020jf005803

Kirby, E., & Ouimet, W. (2011). Tectonic geomorphology along the eastern margin of Tibet: Insights into the pattern and processes of active deformation adjacent to the Sichuan Basin. *Geological Society, London, Special Publications*, *353*(1), 165–188. https://doi.org/10.1144/SP353.9

Koi, T., Hotta, N., Ishigaki, I., Matuzaki, N., Uchiyama, Y., & Suzuki, M. (2008). Prolonged impact of earthquake-induced landslides on sediment yield in a mountain watershed: The Tanzawa region, Japan. *Geomorphology*, *101*(4), 692–702. https://doi.org/10.1016/j.geomorph.2008.03.007

Korup, O. (2012). Earth's portfolio of extreme sediment transport events. *Earth-Science Reviews*, *112*(3–4), 115–125. https://doi.org/10.1016/j.earscirev.2012.02.006

Larsen, I. J., Montgomery, D. R., & Korup, O. (2010). Landslide erosion controlled by hillslope material. *Nature Geoscience*, *3*(4), 247–251. https://doi.org/10.1038/ngeo776

Li, C., Wang, M., Liu, K., & Coulthard, T. J. (2020). Landscape evolution of the Wenchuan earthquake-stricken area in response to future climate change. *Journal of Hydrology*, *590*, 125244. https://doi.org/10.1016/j.jhydrol.2020.125244

Li, G., West, A. J., Densmore, A. L., Hammond, D. E., Jin, Z., Zhang, F., et al. (2016). Connectivity of earthquake-triggered landslides with the fluvial network: Implications for landslide sediment transport after the 2008 Wenchuan earthquake. *Journal of Geophysical Research: Earth Surface*, *121*(4), 703–724. https://doi.org/10.1002/2015JF003718

Li, G., West, A. J., Densmore, A. L., Jin, Z., Parker, R. N., & Hilton, R. G. (2014). Seismic mountain building: Landslides associated with the 2008 Wenchuan earthquake in the context of a generalized model for earthquake volume balance. *Geochemistry, Geophysics, Geosystems*, *15*(4), 833–844. https://doi.org/10.1002/2013GC005067

Li, G., West, A. J., Densmore, A. L., Jin, Z., Zhang, F., Wang, J., et al. (2017). Earthquakes drive focused denudation along a tectonically active mountain front. *Earth and Planetary Science Letters*, *472*, 253–265. https://doi.org/10.1016/j.epsl.2017.04.040

Lin, G.-W., Chen, H., Hovius, N., Horng, M.-J., Dadson, S., Meunier, P., & Lines, M. (2008). Effects of earthquake and cyclone sequencing on landsliding and fluvial sediment transfer in a mountain catchment. *Earth Surface Processes and Landforms*, *33*(9), 1354–1373. https://doi.org/10.1002/esp.1716

Liu-Zeng, J., Zhang, Z., Wen, L., Tapponnier, P., Sun, J., Xing, X., et al. (2009). Co-seismic ruptures of the 12 May 2008, Ms8.0 Wenchuan earthquake, Sichuan: East-west crustal shortening on oblique, parallel thrusts along the eastern edge of Tibet. *Earth and Planetary Science Letters*, *286*(3–4), 355–370. https://doi.org/10.1016/j.epsl.2009.07.017

Ma, C., Wang, Y., Hu, K., Du, C., & Yang, W. (2017). Rainfall intensity–duration threshold and erosion competence of debris flows in four areas affected by the 2008 Wenchuan earthquake. *Geomorphology*, *282*, 85–95. https://doi.org/10.1016/j.geomorph.2017.01.012

Malamud, B. D., Turcotte, D. L., Guzzetti, F., & Reichenbach, P. (2004). Landslides, earthquakes, and erosion. *Earth and Planetary Science Letters*, *229*(1–2), 45–59. https://doi.org/10.1016/j.epsl.2004.10.018

Marc, O., Behling, R., Andermann, C., Turowski, J. M., Illien, L., Roessner, S., & Hovius, N. (2019). Long-term erosion of the Nepal himalayas by bedrock landsliding: The role of monsoons, earthquakes and giant landslides. *Earth Surface Dynamics*, *7*, 107–128. https://doi.org/10.5194/esurf-7-107-2019

Marc, O., & Hovius, N. (2015). Amalgamation in landslide maps: Effects and automatic detection. *Natural Hazards and Earth System Sciences*, *15*(4), 723–733. https://doi.org/10.5194/nhess-15-723-2015

Marc, O., Hovius, N., & Meunier, P. (2016). The mass balance of earthquakes and earthquake sequences. *Geophysical Research Letters*, *43*(8), 3708–3716. https://doi.org/10.1002/2016GL068333

Marc, O., Hovius, N., Meunier, P., Gorum, T., & Uchida, T. (2016). A seismologically consistent expression for the total area and volume of earthquake-triggered landsliding. *Journal of Geophysical Research: Earth Surface*, *121*(4), 640–663. https://doi.org/10.1002/2015JF003732

Marc, O., Hovius, N., Meunier, P., Uchida, T., & Hayashi, S. (2015). Transient changes of landslide rates after earthquakes. *Geology*, *43*(10), 883–886. https://doi.org/10.1130/G36961.1

Marc, O., Stumpf, A., Malet, J., Gosset, M., Uchida, T., & Chiang, S. (2018). Initial insights from a global database of rainfall-induced landslide inventories : The weak influence of slope and strong influence of total storm rainfall. *Earth Surface Dynamics*, *6*, 903–922. https://doi.org/10.5194/esurf-6-903-2018

McGuire, L. A., Kean, J. W., Staley, D. M., Rengers, F. K., & Wasklewicz, T. A. (2016). Constraining the relative importance of raindrop- and flow-driven sediment transport mechanisms in postwildfire environments and implications for recovery time scales. *Journal of Geophysical Research: Earth Surface*, *121*(11), 2211–2237. https://doi.org/10.1002/2016JF003867

Moody, J. A., & Troutman, B. M. (2002). Characterization of the spatial variability of channel morphology. *Earth Surface Processes and Landforms*, *27*(12), 1251–1266. https://doi.org/10.1002/esp.403

Mudd, S. M., Clubb, F. J., Grieve, S. W. D., Milodowski, D. T., Gailleton, B., Hurst, M. D., et al. (2021). *LSDTopoTools2 v0.5* (v0.5). Zenodo [Dataset]. https://doi.org/10.5281/ZENODO.3769703

Ouimet, W. B., Whipple, K. X., & Granger, D. E. (2009). Beyond threshold hillslopes: Channel adjustment to base-level fall in tectonically active mountain ranges. *Geology*, *37*(7), 579–582. https://doi.org/10.1130/G30013A.1

Ouimet, W. B., Whipple, K. X., Royden, L. H., Sun, Z., & Chen, Z. (2007). The influence of large landslides on river incision in a transient landscape: Eastern margin of the Tibetan Plateau (Sichuan, China). *Bulletin of the Geological Society of America*, *119*(11–12), 1462–1476. https://doi.org/10.1130/B26136.1

Pain, C. F., & Bowler, J. M. (1973). Denudation following the November 1970 earthquake. *Zeitschrift Fur Geomorphologie*, *18*, 92–104.

Parker, R. N., Densmore, A. L., Rosser, N. J., De Michele, M., Li, Y., Huang, R., et al. (2011). Mass wasting triggered by the 2008 Wenchuan earthquake is greater than orogenic growth. *Nature Geoscience*, *4*(7), 449–452. https://doi.org/10.1038/ngeo1154

Pearce, A. J., & Watson, A. J. (1986). Effects of earthquake-induced landslides on sediment budget and transport over a 50-yr period. *Geology*, *14*, 52–55. https://doi.org/10.1130/0091-7613(1986)14<52:eoelos>2.0.co;2

Roback, K., Clark, M. K., West, A. J., Zekkos, D., Li, G., Gallen, S. F., et al. (2018). The size, distribution, and mobility of landslides caused by the 2015 Mw7.8 Gorkha earthquake, Nepal. *Geomorphology*, *301*, 121–138. https://doi.org/10.1016/j.geomorph.2017.01.030

Royden, L. H., Burchfiel, B. C., & van der Hilst, R. D. (2008). The geological evolution of the Tibetan plateau. *Science*, *321*(5892), 1054–1058. https://doi.org/10.1126/science.1155371

Santi, P. M., & Morandi, L. (2013). Comparison of debris-flow volumes from burned and unburned areas. *Landslides*, *10*(6), 757–769. https://doi.org/10.1007/s10346-012-0354-4

Schmidt, K. M., & Montgomery, D. R. (1995). Limits to relief. *Science*, *270*(5236), 617–620. https://doi.org/10.1126/science.270.5236.617

Schwanghart, W., Bernhardt, A., Stolle, A., Hoelzmann, P., Adhikari, B. R., Andermann, C., et al. (2016). Repeated catastrophic valley infill following medieval earthquakes in the Nepal Himalaya. *Science*, *351*(6269), 147–150. https://doi.org/10.1126/science.aac9865

Shen, P., Zhang, L. M., Fan, R. L., Zhu, H., & Zhang, S. (2020). Declining geohazard activity with vegetation recovery during first ten years after the 2008 Wenchuan earthquake. *Geomorphology*, *352*, 106989. https://doi.org/10.1016/j.geomorph.2019.106989

Stolle, A., Bernhardt, A., Schwanghart, W., Hoelzmann, P., Adhikari, B. R., Fort, M., & Korup, O. (2017). Catastrophic valley fills record large Himalayan earthquakes, Pokhara, Nepal. *Quaternary Science Reviews*, *177*, 88–103. https://doi.org/10.1016/j.quascirev.2017.10.015

Stolle, A., Schwanghart, W., Andermann, C., Bernhardt, A., Fort, M., Jansen, J. D., et al. (2019). Protracted river response to medieval earthquakes. *Earth Surface Processes and Landforms*, *44*(1), 331–341. https://doi.org/10.1002/esp.4517

Tang, C., Van Asch, T. W. J., Chang, M., Chen, G. Q., Zhao, X. H., & Huang, X. C. (2012). Catastrophic debris flows on 13 August 2010 in the Qingping area, southwestern China: The combined effects of a strong earthquake and subsequent rainstorms. *Geomorphology*, *139–140*(August 2010), 559–576. https://doi.org/10.1016/j.geomorph.2011.12.021.2010

Tang, C., & Van Westen, C. J. (2018). *Atlas of Wenchuan-Earthquake geohazards: Analysis of co-seismic and post-seismic geohazards in the area affected by the 2008 Wenchuan Earthquake*. Science Press. Retrieved from https://issuu.com/ceesvanwesten/docs/atlas_of_wenchuan_earthquake_geohaz

Tang, C., Van Westen, C. J., Tanyas, H., & Jetten, V. G. (2016). Analysing post-earthquake landslide activity using multi-temporal landslide inventories near the epicentral area of the 2008 Wenchuan earthquake. *Natural Hazards and Earth System Sciences*, *16*(12), 2641–2655. https://doi.org/10.5194/nhess-16-2641-2016

Tang, C., Zhu, J., Ding, J., Cui, X., Chen, L., & Zhang, J. (2011). Catastrophic debris flows triggered by a 14 August 2010 rainfall at the epicenter of the Wenchuan earthquake. *Landslides*, *8*(4), 485–497. https://doi.org/10.1007/s10346-011-0269-5

Tolorza, V., Mohr, C. H., Carretier, S., Serey, A., Sepúlveda, S. A., Tapia, J., & Pinto, L. (2019). Suspended sediments in Chilean rivers reveal low postseismic erosion after the Maule earthquake (Mw 8.8) during a severe drought. *Journal of Geophysical Research: Earth Surface*, *124*(6), 1378–1397. https://doi.org/10.1029/2018JF004766

Turowski, J. M., & Rickenmann, D. (2009). Tools and cover effects in bedload transport observations in the Pitzbach, Austria. *Earth Surface Processes and Landforms*, *34*(1), 26–37. https://doi.org/10.1002/esp.1686

Vanmaercke, M., Ardizzone, F., Rossi, M., & Guzzetti, F. (2017). Exploring the effects of seismicity on landslides and catchment sediment yield: An Italian case study. *Geomorphology*, *278*, 171–183. https://doi.org/10.1016/j.geomorph.2016.11.010

Vanmaercke, M., Obreja, F., & Poesen, J. (2014). Seismic controls on contemporary sediment export in the Siret river catchment, Romania. *Geomorphology*, *216*, 247–262. https://doi.org/10.1016/j.geomorph.2014.04.008

Wang, J., Jin, Z., Hilton, R. G., Zhang, F., Densmore, A. L., Li, G., & Joshua West, A. (2015). Controls on fluvial evacuation of sediment from earthquake-triggered landslides. *Geology*, *43*(2), 115–118. https://doi.org/10.1130/G36157.1

Wang, W., Godard, V., Liu-Zeng, J., Scherler, D., Xu, C., Zhang, J., et al. (2017). Perturbation of fluvial sediment fluxes following the 2008 Wenchuan earthquake. *Earth Surface Processes and Landforms*, *42*(15), 2611–2622. https://doi.org/10.1002/esp.4210

West, A. J., Hetzel, R., Li, G., Jin, Z., Zhang, F., Hilton, R. G., & Densmore, A. L. (2014). Dilution of10Be in detrital quartz by earthquake-induced landslides: Implications for determining denudation rates and potential to provide insights into landslide sediment dynamics. *Earth and Planetary Science Letters*, *396*, 143–153. https://doi.org/10.1016/j.epsl.2014.03.058

Wilkinson, P. L., Anderson, M. G., & Lloyd, D. M. (2002). An integrated hydrological model for rain-induced landslide prediction. *Earth Surface Processes and Landforms*, *27*(12), 1285–1297. https://doi.org/10.1002/esp.409

Williams, J. G., Rosser, N. J., Kincey, M. E., Benjamin, J., Oven, K. J., Densmore, A. L., et al. (2018). Satellite-based emergency mapping using optical imagery: Experience and reflections from the 2015 Nepal earthquakes. *Natural Hazards and Earth System Sciences*, *18*(1), 185–205. https://doi.org/10.5194/nhess-18-185-2018

Yang, F., Fan, X., Siva Subramanian, S., Dou, X., Xiong, J., Xia, B., et al. (2021). Catastrophic debris flows triggered by the 20 August 2019 rainfall, a decade since the Wenchuan earthquake. *Landslides*, *18*(9), 1–16. https://doi.org/10.1007/s10346-021-01713-6

Yanites, B. J., Tucker, G. E., Mueller, K. J., & Chen, Y.-G. (2010). How rivers react to large earthquakes: Evidence from central Taiwan. *Geology*, *38*(7), 639–642. https://doi.org/10.1130/G30883.1

Yunus, A. P., Fan, X., Tang, X., Jie, D., Xu, Q., & Huang, R. (2020). Decadal vegetation succession from MODIS reveals the spatio-temporal evolution of post-seismic landsliding after the 2008 Wenchuan earthquake. *Remote Sensing of Environment*, *236*(October 2019), 111476. https://doi.org/10.1016/j.rse.2019.111476

Zhang, F., Jin, Z., West, A. J., An, Z., Hilton, R. G., Wang, J., et al. (2019). Monsoonal control on a delayed response of sedimentation to the 2008 Wenchuan earthquake. *Science Advances*, *5*(6), eaav7110. https://doi.org/10.1126/sciadv.aav7110

Zhang, S., & Zhang, L. M. (2017). Impact of the 2008 Wenchuan earthquake in China on subsequent long-term debris flow activities in the epicentral area. *Geomorphology*, *276*, 86–103. https://doi.org/10.1016/j.geomorph.2016.10.009